RSC Advances

PAPER

View Article Online
View Journal | View Issue

Cite this: *RSC Adv.*, 2017, **7**, 19197

Significant enhancement of visible light photocatalytic activity of the hybrid B_{12}-PIL/rGO in the presence of $Ru(bpy)_3^{2+}$ for DDT dehalogenation

Ying Sun,[a] Wei Zhang,*[a] Jian Tong,[a] Yu Zhang,[a] Shuyao Wu,[a] Daliang Liu,[a] Hisashi Shimakoshi,[b] Yoshio Hisaeda[b] and Xi-Ming Song *[a]

Received 19th February 2017
Accepted 20th March 2017

DOI: 10.1039/c7ra02062g

rsc.li/rsc-advances

A new B_{12}-PIL/rGO hybrid was prepared successfully through immobilizing a B_{12} derivative on the surface of poly(ionic liquid) (PIL)-modified reduced graphene oxide (rGO) by electrostatic attraction and π–π stacking attraction among the different components. The hybrid catalyst showed an enhanced photocatalytic activity in the presence of $Ru(bpy)_3^{2+}$ for 1,1-bis(4-chlorophenyl)-2,2,2-trichloroethane (DDT) dechlorination with ~100% conversion. Especially, the yield of didechlorinated products could reach 78% after 1 h of visible light irradiation, which should be attributed to a synergistic effect of B_{12}, rGO and PIL in B_{12}-PIL/rGO, including their respective catalytic performance, the excellent electron transport of rGO and the concentration of DDT and 1,1-bis(4-chlorophenyl)-2,2-dichloroethane (DDD) on the surface of B_{12}-PIL/rGO. Furthermore, the hybrid catalyst was easily recycled for use without obvious loss of catalytic activity.

Introduction

Dehalogenation reactions have attracted great interest for their potential application in the treatment of halogenated solvent wastes and also as remedial approaches to remove organochlorine pesticide residues from contaminated soils.[1,2] It has been found that vitamin B_{12} and its derivatives could be used as efficient dehalogenation catalysts since they can form Co(I) species which are supernucleophiles and can react with an alkyl halide to form Co(III)–alkyl intermediates.[3–6] Aiming to establish more effective, green and reusable catalytic systems for dehalogenation, some hybrid catalysts fabricated by immobilizing B_{12} derivatives on a matrix for photocatalytic dehalogenation have been reported in recent years.[7–12] In 2009, the Hisaeda group[9] synthesized a hybrid catalyst, B_{12}–TiO_2, through immobilizing a B_{12} derivative, cobyrinic acid, on the surface of TiO_2. It could effectively dehalogenate various organic halides, such as DDT, DDD, and phenethyl bromide, under UV light irradiation (365 nm). In this catalytic system, TiO_2 acted as a photosensitizer and supernucleophilic Co^I was formed by electron transfer from TiO_2 during light irradiation. In order to fully utilize solar energy, we subsequently prepared two copolymer catalysts through immobilizing a B_{12} derivative as catalyst and $[Ru(bpy)_3]^{2+}$ as photosensitizer on the same polymer backbone, namely polystyrene and poly(ionic liquid),[7,11] which could allow efficient electron transfer from the $Ru(bpy)_3^{2+}$ moiety to the cobalt center in the B_{12} complex. However, these soluble polymer catalysts are difficult separate from the catalytic system.

Graphene as a novel carbon-based nanomaterial has been investigated in many fields including catalysis,[13,14] drug delivery,[15] biosensors,[16] photochemical devices[17] and energy storage.[18] In recent years, some hybrid catalysts based on graphene have been shown to exhibit high catalytic activities in photocatalytic reactions such as photocatalytic decomposition of organic pollutants, photocatalytic reduction of CO_2 and splitting of H_2O[19–21] due to graphene's excellent conductivity, superior electron mobility, large surface to volume ratio, high chemical stability and so on.[22–26] To our knowledge, B_{12} in combination with graphene for dehalogenation reactions has not been reported. Here, a novel B_{12}-based hybrid catalyst (B_{12}-PIL/rGO) was prepared, as shown in Fig. 1, by immobilizing a B_{12} derivative on the surface of poly(ionic liquid) (PIL)-modified reduced graphene oxide (rGO) through electrostatic attraction, where the PIL was utilized as a stabilizer to avoid the aggregation of rGO sheets and also made the surface of rGO sheets partly positively charged,[27,28] and then its photocatalytic activity was investigated for DDT dechlorination reaction in the presence of the photosensitizer $Ru(bpy)_3^{2+}$ under visible light irradiation.

Experimental section

Materials

Flake graphite (99.95% purity, average diameter of 1 μm) was purchased from Qingdao Xiyou Graphite Co. Ltd. 1,1-Bis(4-chlorophenyl)-2,2,2-trichloroethane (DDT) and $Ru(bpy)_3Cl_2$ were purchased from J & K Scientific Ltd. Cyanoaqua cobyrinic

[a]*Liaoning Key Laboratory for Green Synthesis and Preparative Chemistry of Advanced Materials, College of Chemistry, Liaoning University, Shenyang 110036, P. R. China. E-mail: weizhanghx@lnu.edu.cn; songlab@lnu.edu.cn; Fax: +86-24-62207922; Tel: +86-24-62207792*

[b]*Department of Chemistry and Biochemistry, Graduate School of Engineering, Kyushu University, Motooka, Fukuoka 819-0395, Japan*

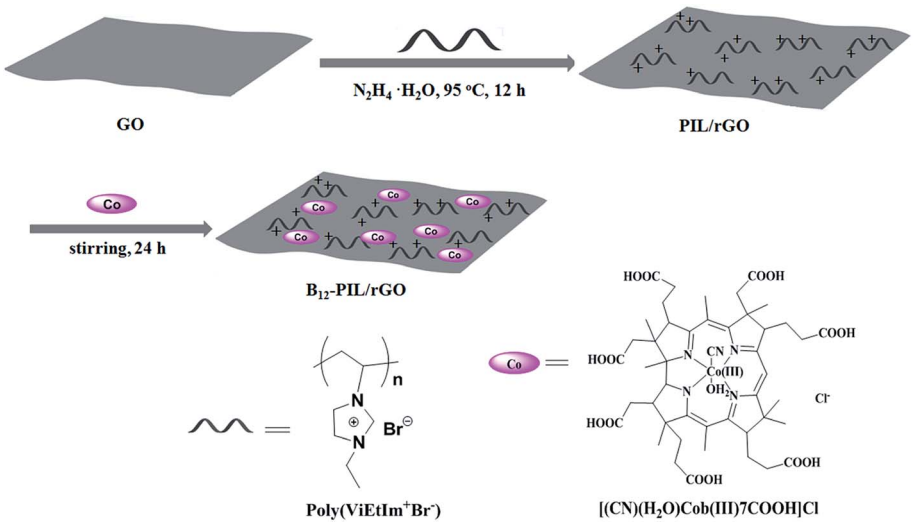

Fig. 1 Illustration of the preparation of the B_{12}-PIL/rGO hybrid.

acid [(CN)(H_2O)Cob(III)7COOH]Cl was synthesized according to the literature.[9] Graphene Oxide (GO) was prepared using a modified Hummers' method as described in our previous work.[17] 1-Vinyl-3-ethylimidazolium bromide (ViEtIm$^+$Br$^-$) and poly(ViEtIm$^+$Br$^-$) were synthesized according to the literature.[29]

Characterizations

The FT-IR spectra were recorded with a PerkinElmer 1600 FT-IR spectrophotometer. The UV-visible spectra were obtained with a PerkinElmer Lambda 25 spectrophotometer. The NMR spectra were recorded with a Mercury Vx-300 MHz NMR spectrometer. The SEM images and EDS analysis were acquired using a Hitachi SU-8010 equipped with an EDX analyzer operated at an accelerating voltage of 15 kV. The TEM images were obtained with a JEM 2100 operating at 200 kV. XRD patterns were obtained with a Bruker D8-Advance. Raman spectra were obtained using a Renishaw inVia Raman microscope with excitation laser wavelength at 633 nm.

Preparation of PIL/rGO nanosheets

GO (100 mg) was dispersed in aqueous solution (100 mL) containing poly(ViEtIm$^+$Br$^-$) (1 g) by sonication, and then hydrazine hydrate (0.2 mL) was added. After the mixture was stirred at 95 °C for 12 h, the composite PIL/rGO was obtained by centrifugation. Then it was washed with distilled water three times to remove the excess poly(ViEtIm$^+$Br$^-$) and dried in vacuum for 24 h.

Preparation of B_{12}-PIL/rGO

[(CN)(H_2O)Cob(III)7COOH]Cl (30 mg) was added to 30 mL aqueous dispersion of PIL/rGO (50 mg) and the mixture was stirred at room temperature for 12 h. Then B_{12}-PIL/rGO nanosheets were obtained after centrifugation and washed with distilled water three times.

General catalytic procedure

A 5 mL methanol solution containing B_{12}-PIL/rGO (3 mg), DDT (2.4×10^{-3} M), $Ru(bpy)_3Cl_2$ (5.5×10^{-4} M) and triethanolamine (0.2 M) was degassed after three freeze–pump–thaw cycles. Then the solution was irradiated for 1 h using a xenon lamp with a $\lambda > 400$ nm optical filter and a heat cut-off filter. After removing the solvent by evaporation, the residue was washed with hexane three times and the products and the unreacted substrate were dissolved in hexane. After removing the solvent, a white solid was obtained and analyzed by ^{1}H NMR using 1,4-dioxane as the internal standard. The B_{12}-PIL/rGO hybrid catalyst was washed with methanol, and then reused after adding fresh triethanolamine, $Ru(bpy)_3Cl_2$ and the substrate.

Results and discussion

Preparation and characterization of B_{12}-PIL/rGO nanosheets

Fig. 1 illustrates the preparation procedure for B_{12}-PIL/rGO. GO was reduced to rGO by hydrazine hydrate in poly(ViEtIm$^+$Br$^-$) aqueous solution and the PIL/rGO composite was fabricated directly in the suspension because of the electrostatic and π–π interactions between rGO and poly(ViEtIm$^+$Br$^-$). The B_{12} derivative [(CN)(H_2O)Cob(III)7COOH]Cl was subsequently fixed on the surface of the PIL/rGO nanosheets through electrostatic self-assembly between imidazolium cations and the B_{12} derivative after it was added to the suspension. High dispersity of a catalyst can effectively improve its catalytic activity for a heterogeneous catalytic system, and thus the dispersity of the hybrid in each of water and methanol was evaluated. Compared to rGO, this hybrid exhibited improved dispersity in water and methanol due to the introduction of PIL and the water-soluble B_{12} derivative on the surface of rGO. As shown in Fig. 2, the dispersion of B_{12}-PIL/rGO in methanol possessed high stability, while almost all the rGO settled out from the dispersion after standing for 1 h.

The preparation procedure of the hybrid was monitored by zeta potential measurements. Fig. 3 shows the zeta potential data of GO (a), PIL/rGO (b) and B_{12}-PIL/rGO (c) in 0.1 M PBS (pH = 7.0). The zeta potential of GO is around −38.5 mV. After GO was reduced to rGO and further modified by the cationic PIL,

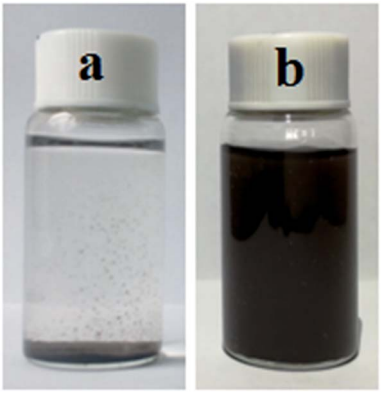

Fig. 2 Photographs of rGO (a) and B_{12}-PIL/rGO (b) dispersions in methanol after standing for 1 h at room temperature.

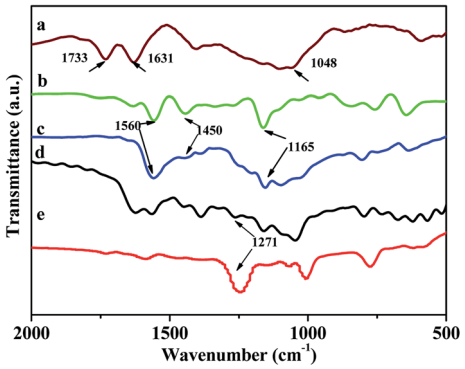

Fig. 4 FT-IR spectra of GO (a), poly(ViEtIm$^+$Br$^-$) (b), PIL/rGO (c), B_{12}-PIL/rGO (d) and B_{12} catalyst (e).

the zeta potential of the obtained PIL/rGO significantly moves to +42.4 mV. The obvious decrease of the zeta potential of B_{12}-PIL/rGO at +19.4 mV should be attributed to the introduction of the B_{12} derivative. The change of the surface charge in the hybrid could further indicate that PIL and B_{12} complex were successfully grafted onto the rGO surface.

The FT-IR spectra of GO, poly(ViEtIm$^+$Br$^-$), PIL/rGO, the B_{12} derivative and the resulting B_{12}-PIL/rGO are shown in Fig. 4. The appearance of characteristic absorption peaks at 1733, 1631 and 1048 cm^{-1} (stretching vibrations of C=O, C=C and C–O, respectively) revealed the presence of C=O, C=C and C–O functional groups in GO. While in the spectrum of PIL/rGO, the peak at 1733 cm^{-1} assigned to the C=O stretch of the carboxylic group of GO completely disappears which proves that GO was reduced by hydrazine hydrate. The characteristic peaks of imidazolium cations at 1560, 1450 and 1165 cm^{-1} in the spectrum of PIL/rGO indicate that poly(ViEtIm$^+$Br$^-$) was assembled onto the surface of rGO nanosheets successfully. After the B_{12} derivative was adsorbed on PIL/rGO, the spectrum of the obtained B_{12}-PIL/rGO presents the typical absorption bands at 1271 cm^{-1} from the B_{12} derivative. These observations also indicate that the B_{12} derivative was assembled onto the surface of the PIL/rGO nanosheets.

Fig. 5 shows the UV-visible spectra of B_{12}-PIL/rGO, GO, PIL/rGO and B_{12} in water. GO exhibits a typical absorption at 228 nm assigned to the π–π^* transition of C=C band. In the spectrum of PIL/rGO, this transition absorption peak is red-shifted to 270 nm, which is attributed to the deoxygenation and partial restoration of the electronic conjugation after the reduction process. Poly(ViEtIm$^+$Br$^-$) does not show an obvious absorption in the range of 200–800 nm, which coincides with the literature.[29] The B_{12} derivative exhibits three typical absorption peaks at 352, 497 and 529 nm.[9] Therefore, in the case of B_{12}-PIL/rGO, the characteristic absorption peaks at 360, 515 and 547 nm should be assigned to the B_{12} derivative. The UV-visible spectra further prove the successful preparation of the B_{12}-PIL/rGO hybrid.

Dry B_{12}-PIL/rGO, PIL/rGO, rGO and GO powders were each used in the XRD analysis, as shown in Fig. 6. The XRD analysis indicates that the interlayer spacing of rGO ($2\theta = 24.5°$, 0.363 nm) decreases obviously compared to that of GO ($2\theta = 11.6°$, 0.762 nm), as a result of the removal of oxygen-containing groups from the carbon sheets. Compared with rGO, the diffraction peak of PIL/rGO shifted to $2\theta = 23.2°$, indicating the slight broadening of interlayer spacing to 0.383 nm due to the introduction of PIL. After the B_{12} derivative was further

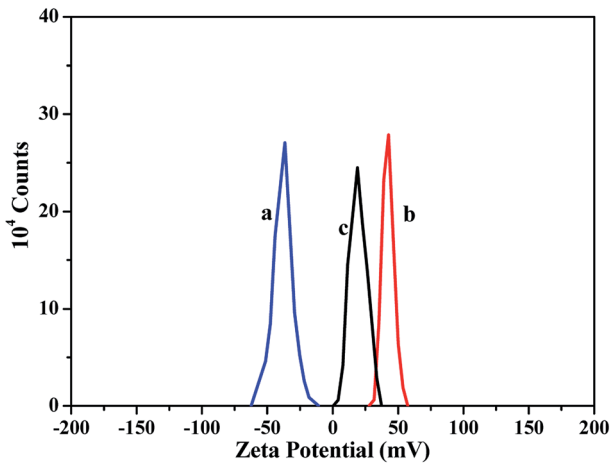

Fig. 3 Zeta potential distributions of GO (a), PIL/rGO (b) and B_{12}-PIL/rGO (c) in 0.1 M PBS (pH = 7.0).

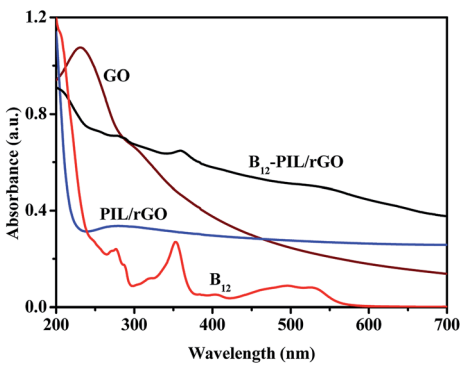

Fig. 5 UV-visible spectra of B_{12}-PIL/rGO, GO, PIL/rGO and B_{12} in water.

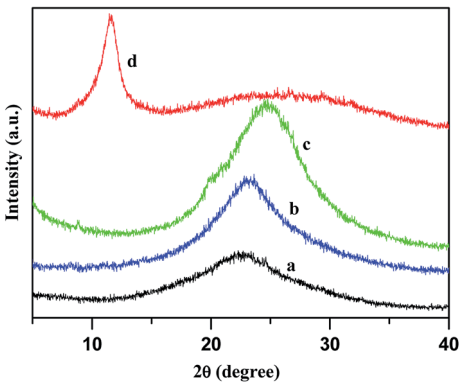

Fig. 6 XRD patterns of B_{12}-PIL/rGO (a), PIL/rGO (b), rGO (c) and GO (d).

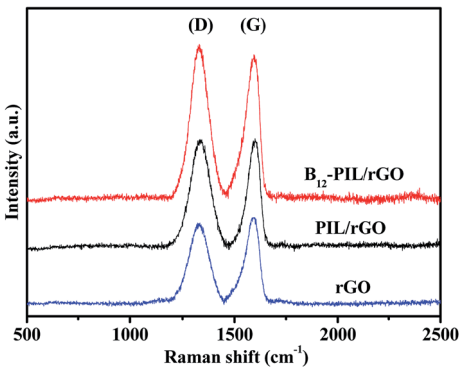

Fig. 7 Raman spectra of rGO, PIL/rGO and B_{12}-PIL/rGO.

decorated on the PIL/rGO sheets, the diffraction peak of B_{12}-PIL/rGO shifted to $2\theta = 22.4°$, corresponding to an interlayer spacing of 0.397 nm.

Raman spectroscopy is usually employed to provide structural information for carbon materials. Fig. 7 shows the Raman spectra of rGO, PIL/rGO and B_{12}-PIL/rGO. As shown in Fig. 7, rGO shows a disorder-induced D band at 1341 cm^{-1} and a G band at 1597 cm^{-1} resulting from the sp^3-hybridized carbon and the sp^2-hybridized carbon respectively.[29,30] In comparison with rGO, the D and G bands of the PIL/rGO hybrid are slightly shifted to 1330 and 1593 cm^{-1} respectively, proving the existence of interaction between PIL and rGO. In addition, the I_D/I_G ratios of rGO, PIL/rGO and B_{12}-PIL/rGO gradually increase and are 0.93, 1.01 and 1.05 respectively, reflecting the increasing disorder in the PIL/rGO and B_{12}-PIL/rGO hybrids attributed to the introduction of PIL and the B_{12} derivative on the surface of rGO.

The chemical compositions of PIL/rGO and B_{12}-PIL/rGO nanosheets were determined by EDS (Fig. 8). Amounts of 62.77% of C, 19.34% of O, 16.27% of N and 1.62% of Br were found in the PIL/rGO nanosheets, where the N and Br peaks arose from the imidazole cations and the counter ions of poly(ViEtIm$^+$Br$^-$) respectively, the O peak originated from rGO and the C peak originated from both rGO and poly(ViEtIm$^+$Br$^-$). In the spectrum of B_{12}-PIL/rGO, besides C, O, N and Br peaks, an amount of 0.70% of Co was also detected which should derive from B_{12}, and the decrease of Br from 1.62% to 0.34% should be attributed to the part anionic exchange with B_{12}.

The morphologies of GO and B_{12}-PIL/rGO were characterized by SEM and TEM. It was found that GO possessed layered structures with crumpled or wrinkled sheets (Fig. 9A and C). Compared with GO, B_{12}-PIL/rGO (Fig. 9B and D) displayed thicker and fewer wrinkled layers, indicating that the structure of the rGO had not changed after modification.

The catalytic performance of the hybrid catalyst B_{12}-PIL/rGO

The visible light photocatalytic activity of B_{12}-PIL/rGO was investigated using DDT as a substrate in the presence of the photosensitizer $Ru(bpy)_3Cl_2$ in methanol. The results are summarized in Table 1. For the B_{12}-PIL/rGO hybrid in the presence of $Ru(bpy)_3Cl_2$, DDT was almost completely converted to dechlorinated products including 1,1-bis(4-chlorophenyl)-2,2-dichloroethane (DDD, 58% yield), 1-bis(4-chlorophenyl)-2-chloroethane (DDMS, 5% yield), 1,1,4,4-tetrakis(4-chlorophenyl)-2,3-dichloro-2-butene (TTDB (E/Z), 8% yield) and 1,1-bis(4-chlorophenyl)-2-chloroethylene (DDMU, 10% yield) after 20 min of visible light irradiation (entry 2 in Table 1). According to the reported formation mechanism of the products of DDT dechlorination, TTDB (E/Z) is the product of coupling reaction between two didechlorinated carbene intermediates.[31] Therefore, the total yield of didechlorinated products for this catalytic system was 31%. When the irradiation time was increased

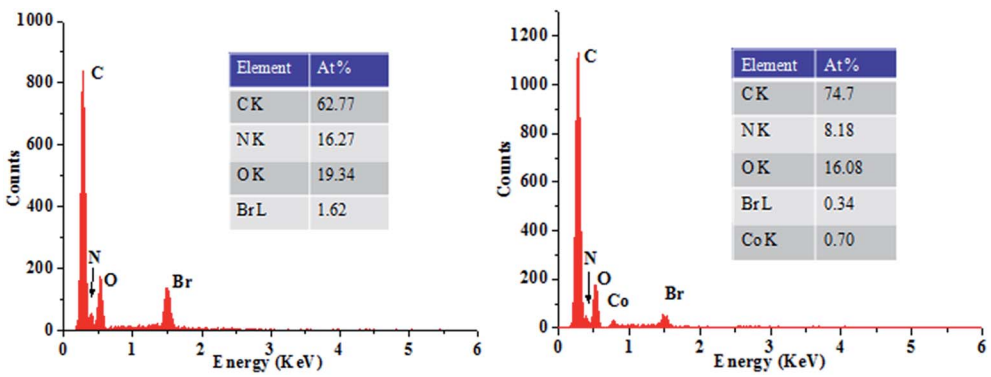

Fig. 8 EDS spectra of PIL/rGO (left) and B_{12}-PIL/rGO (right).

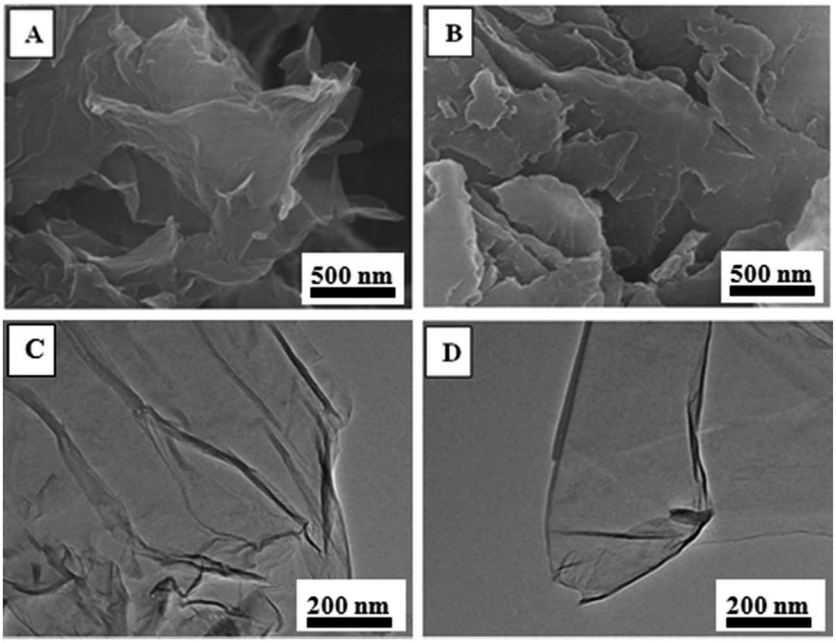

Fig. 9 SEM images of GO (A) and B_{12}-PIL/rGO (B); TEM images of GO (C) and B_{12}-PIL/rGO (D).

Table 1 Photocatalytic dechlorination of DDT catalyzed by B_{12}-PIL/rGO[a]

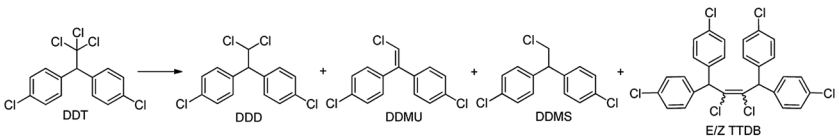

Entry	Catalyst and photosensitizer	Irradiation time (min)	Conversion (%)	Product yield[b] (%)			
				DDD	DDMS	TTDB (E/Z)	DDMU
1	B_{12}-PIL/rGO, $Ru(bpy)_3Cl_2$	10	43	26	Trace	6	2
2	B_{12}-PIL/rGO, $Ru(bpy)_3Cl_2$	20	99	58	5	8	10
3	B_{12}-PIL/rGO, $Ru(bpy)_3Cl_2$	60	≈100	21	14	16	32
4[c]	B_{12}-PIL/rGO, $Ru(bpy)_3Cl_2$	—	Trace	—	—	—	—
5	Only $Ru(bpy)_3Cl_2$	60	33	18	—	—	—
6	Only B_{12}-PIL/rGO	60	29	11	—	—	—
7[d]	B_{12}, $Ru(bpy)_3Cl_2$	60	68	65	—	—	—
8[e]	PIL/rGO, $Ru(bpy)_3Cl_2$	60	77	70	—	—	—

[a] B_{12}-PIL/rGO = 3 mg, $[DDT] = 2.4 \times 10^{-3}$ M, $[Ru(bpy)_3Cl_2] = 5.5 \times 10^{-4}$ M, [TEOA] = 0.2 M, irradiation $\lambda \geq 400$ nm, 50 mW cm^{-2}, distance: 10 cm. [b] DDT conversion and the product yields were determined by ^1H NMR. [c] The reaction was kept in the dark for 60 min. [d] $[B_{12}] = 3$ mg. [e] PIL/rGO = 3 mg.

to 60 min (entry 3 in Table 1), the total yield of the didechlorinated products increased to 78% while the DDD yield decreased to 21%. The reaction did not proceed under dark conditions (entry 4 in Table 1). When only $Ru(bpy)_3Cl_2$ or B_{12}-PIL/rGO (entries 5 and 6 in Table 1) was used, the DDT conversion rates were 33 and 29% respectively. In contrast to the result for the hybrid system (entry 3), the conversion rate of DDT was 68% and no didechlorinated products were obtained even after 60 min of irradiation when a mixture of the B_{12} derivative ([(CN)(H_2O)Cob(III)7COOH]Cl) and $Ru(bpy)_3Cl_2$ was used, where 3 mg B_{12} catalyst was directly used instead of 3 mg B_{12}-PIL/rGO (entry 7 in Table 1). When using PIL/rGO instead of B_{12}-PIL/rGO in the presence of $Ru(bpy)_3Cl_2$ (entry 8 in Table 1), the DDT conversion reached 77% with DDD as the single product after 60 min of irradiation. This result indicated that rGO which has excellent electroconductivity[32] could transfer electrons to DDT and reduce it to DDD after it accepted electrons from the photosensitizer $Ru(bpy)_3^{2+}$ under visible light irradiation.[33] At the same time, the fact that no didechlorinated products were obtained without B_{12} in the hybrid fully proved that B_{12} was essential for didechlorination.

It is well known that removing the second chlorine atom is much more difficult than the first one from DDT molecules. According to the literature, for B_{12}-based photocatalysts, B_{12}-BVIm-Ru copolymer[7] and B_{12}-HAS artificial enzyme,[34] which are comparable to that used in this work, although they all showed enhanced photocatalytic activities with ~100% conversion of DDT, few didechlorinated products were detected. From the above comparison, it can be concluded that the B_{12}-PIL/rGO hybrid possessed very high photocatalytic activity for DDT dechlorination, especially for its didechlorination, in the presence of the photosensitizer $Ru(bpy)_3Cl_2$, and the introduction of rGO significantly enhanced the reaction efficiency.

In order to further investigate the dechlorination process of DDT and the role of rGO in the hybrid catalytic system, the reaction was performed under shorter irradiation time. When the irradiation time was shortened to 10 min, DDT conversion decreased obviously to 43% (entry 1 in Table 1) and the didechlorinated products DDMU and TTDB (E/Z) were also found except DDD. This result fully proved that some DDD molecules were further dechlorinated quickly once one chloride atom was removed from the structure of DDT to produce DDD catalyzed by B_{12} catalyst or rGO in this hybrid catalytic system. Therefore, it is reasonable to deduce that this excellent catalytic efficiency should be attributed to the introduction of rGO which played a very important role not only as an electron mediator but also as one of the catalysts catalyzing DDT dechlorination to DDD in the current system, and a synergistic effect of B_{12}, rGO and PIL in B_{12}-PIL/rGO, including their respective catalytic performance, the excellent electron transport of rGO and the concentration of DDT and DDD on the surface of B_{12}-PIL/rGO, accelerated the dechlorination reactions of DDT and DDD.

According to the literature,[31,35] a plausible mechanism of this catalytic system is shown in Fig. 10. Firstly, the photosensitizer $Ru(II)(bpy)_3^{2+}$ was excited by visible light irradiation, forming its excited state $Ru(II)(bpy)_3^{2+}*$. Then the excited species was quenched by sacrificial triethanolamine (TEOA) to form $Ru(bpy)_3^{+}$ and the obtained $Ru(bpy)_3^{+}$ transferred an electron to the rGO sheets. Subsequently, the Co(III) center of the B_{12} derivative in the hybrid accepted two electrons from rGO sheets and was reduced to form the Co(I) species. The supernucleophilic Co(I) species had a high reactivity with organic halides to induce the oxidative addition of the alkylating agents to the metal center with dehalogenation. Finally, the resulting Co(III)–alkyl complex proceeded to homolytic Co–C bond cleavage to form the Co(II) species and an alkyl radical, which could accept a proton from the medium or couple or rearrange to give the corresponding products. In the catalytic system (in Fig. 10), some of the $Ru(bpy)_3^{2+}$ moieties can be adsorbed reversibly on the surface of rGO due to the electrostatic interaction and weak π–π interaction between them, and thus rGO can easily accept electrons from the Ru complex under irradiation and subsequently rapidly transfer them to the Co center of the B_{12} complex on its surface.

Furthermore, the recycled catalysis of the B_{12}-PIL/rGO hybrid catalyst was performed since it can be easily separated from the reaction system by centrifugation. The relevant data are shown in Table 2. According to the data, the hybrid catalyst still kept high catalytic activity in the third run under 60 min of irradiation. The recyclability of the B_{12}-PIL/rGO hybrid catalyst at lower

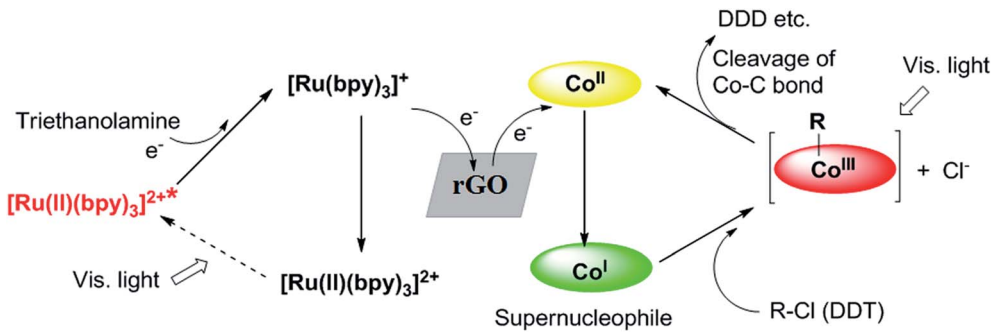

Fig. 10 Proposed mechanism for DDT dechlorination.

Table 2 Recycled catalysis of B_{12}-PIL/rGO[a]

Entry	Irradiation time (min)	Cycle	Conversion (%)	Product yield[b] (%)			
				DDD	DDMS	TTDB (E/Z)	DDMU
1	60	1	100	21	14	16	32
		2	99	21	13	15	31
		3	98	21	13	15	30
2	10	1	43	26	Trace	6	2
		2	41	25	1	5	3
		3	42	21	Trace	6	3

[a] $[DDT] = 2.4 \times 10^{-3}$ M, $[Ru(bpy)_3Cl_2] = 5.5 \times 10^{-4}$ M, [TEOA] = 0.2 M, irradiation $\lambda \geq 400$ nm, 50 W cm^{-2}, distance: 10 cm. [b] DDT conversion and the product yields were determined by ^{1}H HMR.

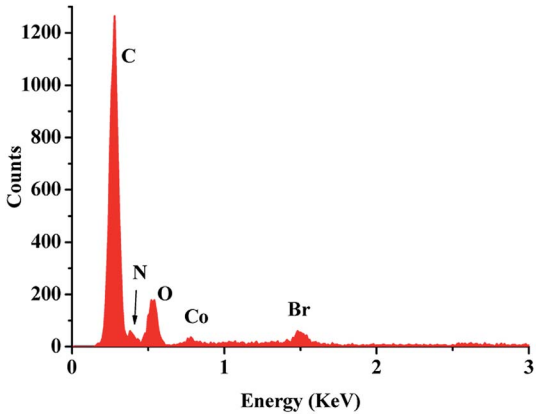

Fig. 11 EDS spectrum of B_{12}-PIL/rGO after 3 recycles.

conversion has also been investigated under 10 min of irradiation (shown in Table 2). These data indicated that this hybrid catalyst had good stability and recyclability, and kept its catalytic activity after 3 recycles even at lower conversion. The recovered B_{12}-PIL/rGO after 3 recycles was characterized by EDS (Fig. 11), showing that the chemical compositions of the hybrid have no distinct change compared with the original.

Conclusions

A rGO-supported B_{12} catalyst was successfully synthesized and its photocatalytic activity was evaluated in the presence of Ru(II) trisbipyridine for DDT dechlorination under visible light irradiation. Using the catalytic system, DDT could be effectively dechlorinated and the yield of didechlorination reached 78% after 1 h of visible light irradiation, which is much higher than that of other reported photocatalytic systems. These results indicate that rGO could act not only as an electron mediator in the hybrid catalyst, but also as a catalyst for the dechlorination reaction and significantly enhance the catalytic efficiency of the hybrid catalytic system. In addition, this hybrid catalyst is environmentally friendly since it can be easily reused without any loss of catalytic efficiency.

Acknowledgements

We are grateful for financial support from Science Foundation of Educational Department of Liaoning Province (LYB201604) and the National Natural Science Foundation of China (51273087).

Notes and references

1 C. Hu, B. Yue and T. Yamase, *Appl. Catal., A*, 2000, **194**, 99.
2 C. A. Crock and V. V. Tarabara, *Environ. Sci.: Nano*, 2016, **3**, 453.
3 H. Shimakoshi, L. Li, M. Nishi and Y. Hisaeda, *Chem. Commun.*, 2011, **47**, 10921.
4 J. Shey and W. A. V. D. Donk, *J. Am. Chem. Soc.*, 2000, **122**, 12403.
5 D. A. Pratt and V. D. D. Wa, *Chem. Commun.*, 2006, **5**, 558.
6 K. M. Mccauley, D. A. Pratt, S. R. Wilson, J. Shey, T. J. Burkey and W. A. V. D. Donk, *J. Am. Chem. Soc.*, 2005, **127**, 1126.
7 W. Zhang, H. Shimakoshi, N. Houfuku, X. M. Song and Y. Hisaeda, *Dalton Trans.*, 2014, **43**, 13972.
8 H. Shimakoshi, M. Abiru, S. Izumi and Y. Hisaeda, *Chem. Commun.*, 2009, **41**, 6427.
9 H. Shimakoshi, E. Sakumori, K. Kaneko and Y. Hisaeda, *Chem. Lett.*, 2009, **38**, 468.
10 H. Shimakoshi, M. Nishi, A. Tanaka, K. Chikama and Y. Hisaeda, *Chem. Lett.*, 2010, **39**, 22.
11 H. Shimakoshi, M. Nishi, A. Tanaka, K. Chikama and Y. Hisaeda, *Chem. Commun.*, 2011, **47**, 6548.
12 D. Zhou, C. K. Njue and J. F. Rusling, *J. Am. Chem. Soc.*, 1999, **121**, 2909.
13 Q. Xiang, J. Yu and M. Jaroniec, *Chem. Soc. Rev.*, 2012, **41**, 782.
14 Y. Liang, Y. Li, H. Wang, J. Zhou, J. Wang, T. Regier and H. Dai, *Nat. Mater.*, 2011, **10**, 780.
15 S. Goenka, V. Sant and S. Sant, *J. Controlled Release*, 2014, **173**, 75.
16 Y. Shao, J. Wang, H. Wu, J. Liu, I. A. Aksay and Y. Lin, *Electroanalysis*, 2010, **22**, 1027.
17 W. Zhang, H. Bai, Y. Zhang, Y. Sun, S. Lin, J. Liu, Q. Yang and X. M. Song, *Mater. Chem. Phys.*, 2014, **147**, 1140.
18 X. Cao, Y. Shi, W. Shi, G. Lu, X. Huang, Q. Yan, Q. Zhang and H. Zhang, *Small*, 2011, **7**, 3163.
19 J. Yu, J. Jin, B. Cheng and M. Jaroniec, *J. Mater. Chem. A*, 2014, **2**, 3407.
20 L. M. Pastrana-Martínez, S. Morales-Torres, J. L. Figueiredo, J. L. Faria and A. M. T. Silva, Graphene Derivatives in Photocatalysis, in *Graphene-based Energy Devices*, Wiley-VCH Verlag GmbH & Co. KGaA, 2015, p. 249.
21 Z. Xu, Z. Ao, D. Chu, A. Younis, C. M. Li and S. Li, *Sci. Rep.*, 2014, **4**, 6450.
22 Y. Zhang, Y. W. Tan, H. L. Stormer and P. Kim, *Nature*, 2005, **438**, 1.
23 C. Lee, X. Wei, J. W. Kysar and J. Hone, *Science*, 2008, **321**, 385.
24 K. S. Novoselov, Z. Jiang, Y. Zhang, S. V. Morozov, H. L. Stormer, U. Zeitler, J. C. Maan, G. S. Boebinger, P. Kim and A. K. Geim, *Science*, 2007, **315**, 1379.
25 D. Chen, H. Zhang, Y. Liu and J. Li, *Energy Environ. Sci.*, 2013, **6**, 1362.
26 S. Wu, Y. Wang, H. Mao, C. Wang, L. Xia, Y. Zhang, H. Ge and X. M. Song, *RSC Adv.*, 2016, **6**, 59487.
27 H. Zhang, X. Lv, Y. Li, Y. Wang and J. Li, *ACS Nano*, 2010, **4**, 380.
28 X. Zhou, T. Wu, K. Ding, B. Hu, M. Hou and B. Han, *Chem. Commun.*, 2010, **46**, 386.
29 J. W. Liu, M. M. Wang, Y. Zhang, L. Han, X. W. Chen and J. H. Wang, *RSC Adv.*, 2014, **4**, 61936.
30 J. Li, Q. Li, Y. Zeng, T. Tang, Y. Pan and L. Li, *RSC Adv.*, 2014, **5**, 717.

31 H. Shimakoshi, M. Tokunaga, T. Baba and Y. Hisaeda, *Chem. Commun.*, 2004, **16**, 1806.
32 A. Iwase, Y. H. Ng, Y. Ishiguro, A. Kudo and R. Amal, *J. Am. Chem. Soc.*, 2011, **133**, 11054.
33 S. Li, X. Zhong, H. Yang, Y. Hu, F. Zhang, Z. Niu, W. Hu, Z. Dong, J. Jin and R. Li, *Carbon*, 2011, **49**, 4239.
34 Y. Hisaeda, K. Tahara, H. Shimakoshi and T. Masuko, *Pure Appl. Chem.*, 2013, **85**, 1415.
35 H. Shimakoshi, S. Kudo and Y. Hisaeda, *Chem. Lett.*, 2005, **34**, 1096.